JMEPEG (2005) 14:765-772
DOI: 10.1361/105994905X75583

1059-9495/$19.00

Fatigue Performance of Metastable β Titanium Alloys: Effects of Microstructure and Surface Finish

Marcin Kocan, H.J. Rack, and Lothar Wagner

(Submitted August 24, 2005)

This investigation examined the role of microstructure and surface finish on the high cycle fatigue (HCF) performance of TIMETAL LCB (Ti-6.8Mo-4.5Fe-1.5Al). The as-received microstructure of LCB consisted of elongated β grains with a semicontinuous grain boundary α layer. In contrast, a fine equiaxed β + spheroidized α LCB microstructure was achieved by hot swaging and solution (recrystallization) anneal. The latter modification of the prior β grain structure, together with the size, morphology, and distribution of the primary α phase, resulted in a significant enhancement in the tensile and HCF properties. Furthermore, prestraining (PS), as would be expected during the fabrication of an automotive coil spring, and prior to aging for 30 min at temperatures between 500 and 550 °C, led to additional increases in tensile strength. In contrast, the HCF performance was always reduced when PS prior to aging was included in the overall processing procedure. Finally, shot-peening and roller-burnishing both resulted in an increased fatigue life in the finite life regimen; however, significant reductions in the 10^7 cycle fatigue strengths were observed when these procedures were used. These observations have been explained by including the effect of process-induced residual tensile stresses in the fatigue analysis, resulting in subsurface fatigue crack nucleation.

Keywords fatigue crack nucleation, residual stress, roller-burnishing, shot-peening

1. Introduction

Metastable β titanium alloys, due to their high specific strengths, low elastic moduli, and high corrosion resistance, are presently being considered as candidates for suspension spring materials (Ref 1-3). Indeed, it has been proposed that the substitution of these alloys for conventional steel springs will result in a weight reduction of approximately 40% (Ref 4). Furthermore, this substitution will eliminate the need to include a corrosion-resistant coating as is presently required for steel springs (Ref 5). This investigation is aimed at optimizing the microstructure of TIMETAL LCB (Ti-6.8Mo-4.5Fe-1.5Al), which is one of prime candidates for suspension spring application. Various methods for altering the microstructure and mechanical behavior of this alloy have been explored.

2. Experimental

The alloy examined in this investigation was received from TIMET (Henderson, NV) as 14.3 mm diameter round rod that had been solution heat-treated (AR) at 760 °C for 20 min followed by fan air cooling. Its chemical composition as determined by TIMET was: 4.5 wt.% Fe, 6.6 wt.% Mo, 1.5 wt.% Al, 0.142 wt.% O, balance Ti. Two processing procedures were examined. The first involved aging of the AR alloy for various times and temperatures between 500 and 550 °C with and without prior tensile prestraining (PS). The second involved resolution heat treatment and swaging at 760 °C to a 50% reduction of the cross section followed by a recrystallization anneal at 760 °C for 30 min. This recrystallized (RX) material was aged under conditions similar to those of the original solution-treated material, again with and without tensile PS.

The degree of tensile PS prior to aging was furthermore varied between 0% and 10%, the latter representing a typical maximum surface strain that is expected during the winding of a coil spring. The magnitude of this surface strain was estimated from $\varepsilon_{max}| = |d/D$, with d equal to the rod diameter, D equal to the coil spring diameter, and d and D being taken as 10 and 100 mm, respectively.

It should, however, be recognized that this methodology only approximates the performance of an actual coil spring; the aging of the spring will actually result in a graded material. This gradient is a consequence of the winding operation during which an elastic-plastic strain gradient will be established through the coiled rod. Upon aging, precipitation of α will occur, with the extent of this precipitation, for example, the volume fraction, size, and spacing of the α particles, being a function of the degree of PS. Higher PS, as experienced at the coil surface, result in a higher volume fraction and a finer α distribution (Ref 6). In contrast, the center of the rod will undergo little or no strain.

Following aging, tensile tests were performed on threaded cylindrical specimens having a gage length and gage diameter

This paper was presented at the Beta Titanium Alloys of the 00's Symposium sponsored by the Titanium Committee of TMS, held during the 2005 TMS Annual Meeting & Exhibition, February 13-16, 2005 in San Francisco, CA.

Marcin Kocan and **Lothar Wagner,** Institute of Materials Science and Engineering, Clausthal University of Technology, Agricolastrasse 6, 38678 Clausthal-Zellerfeld, Germany; and **H.J. Rack,** School of Materials Science and Engineering, Clemson University, 213 Olin Hall, Clemson, SC 29634. Contact e-mail: rackh@clemson.edu.

of 20 and 4 mm, respectively. Additionally, high cycle fatigue (HCF) tests were performed on electropolished (EP) hourglass-shaped specimens (minimum diameter 3.0 mm) in rotating beam loading ($R = -1$) at frequencies of 50 Hz in air. Other complementary specimens were shot-peened to an Almen intensity (mmA) of 0.55 mmA using spherically conditioned cut wire made of quenched and tempered steel (average diameter 0.6 mm, HV 0.1 800). Finally, a third group was roller-burnished using a hydraulically driven hard metal ball (diameter 6 mm) applied at a rolling force of 550 N, with both the spot-peening and roller-burnishing conditions based on a prior study (Ref 7). Following failure, selected fracture surfaces were examined by scanning electron microscopy (SEM).

After shot-peening (SP) and roller-burnishing, the change in surface layer properties was evaluated by microhardness and residual stress-depth profiles; the latter were determined by the incremental hole-drilling technique, as described elsewhere (Ref 8). In addition, the surface topography was measured by a profilometer.

3. Results and Discussion

3.1 Microstructures

The microstructures of the original AR and RX conditions are illustrated in Fig. 1. Figure 1(a) shows the primary α grains (dark) that surround the β grains (light), which were elongated in the longitudinal direction of the rods. This direction corresponds to the flow direction of the prior work. A comparison of Fig. 1(a) and (b) also shows that increasing the solution time from 20 min (AR) to 50 min (AR + SHT) resulted in an increase in the β grain size and partial spheroidization of the α phase. In contrast, swaging plus recrystallization

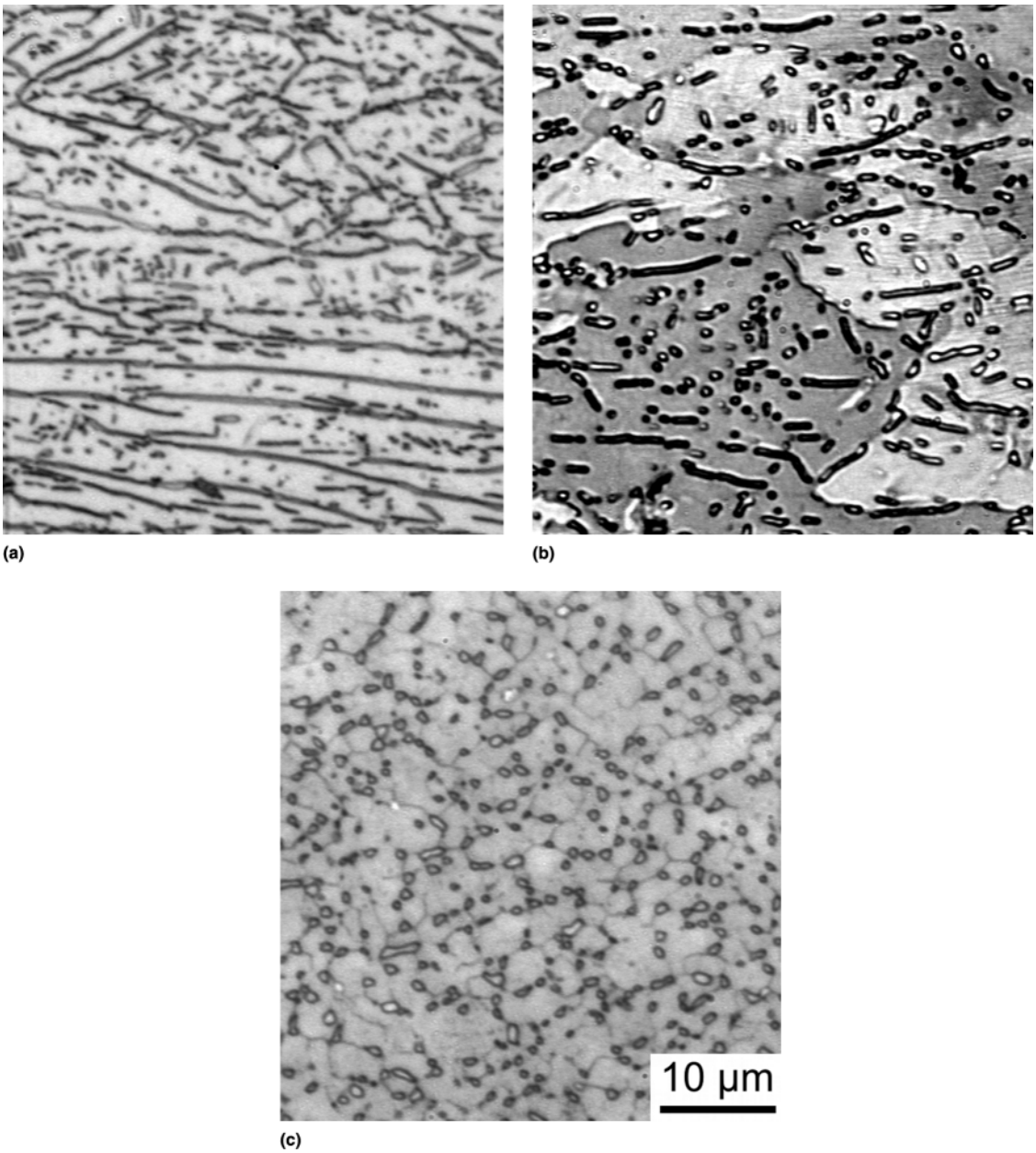

Fig. 1 Microstructures of LCB material: (a) AR; (b) AR + SHT; and (c) RX

(RX) (Fig. 1c) resulted in a fine equiaxed β grain structure with almost complete spheroidization of the primary α phase.

3.2 Tensile Properties

The tensile properties of the unaged conditions examined in this study are summarized in Table 1. The data show that the yield stress (YS), tensile strength, and ductility all decreased as the solution-annealing time increased (i.e., AR versus AR + SHT). Additionally, as the β grain size decreased and the degree of primary α spheroidization increased (i.e., AR + SHT versus RX) the yield and ultimate strengths, as well as the true fracture strain (ε_F), increased. This change can be ascribed to the decrease in slip length occasioned by the aforementioned microstructure refinement (compare Fig. 1a-c).

The influence of PS and aging on the tensile properties of RX LCB is illustrated in Table 2. Prestraining without subsequent aging led to a slight increase in strength. The low level of increase was associated with the low work-hardening capability of metastable β titanium alloys. Prestraining followed by aging at 500 °C for 0.5 h resulted, however, in YS and ultimate tensile strengths (UTS) that were markedly higher than those of material aged without PS. While an increase in aging time from 0.5 to 4 h at 500 °C slightly decreased the strength values of material with no PS, the same increase in aging time led to a drastic loss of the strength values and a concomitant pronounced increase in the ductility of prestrained material (Table 2). This effect of PS on the kinetics of α precipitation is consistent with prior efforts on other metastable β alloys (Ref 9, 10). Ultimately, aging at temperatures above 500 °C resulted in a decrease in strength, with a concomitant increase in tensile ductility (Fig. 2) as already reported in Ref 11 and 12.

Table 1 Tensile properties of TIMET LCB (SHT conditions)

Properties	E, GPa	$\sigma_{0.2}$, MPa	UTS, MPa	e_u, %	El, %	RA, %	$\varepsilon_F = \ln(A_0/A_F)$
AR	89	1090	1100	12.0	20.0	46.5	0.63
AR + SHT	86	1020	1030	12.0	18.0	40.5	0.52
RX	81	1110	1110	10.0	19.5	53.5	0.77

3.3 High Cycle Fatigue Properties (Electropolished Conditions)

3.3.1 Influence of Primary α Spheroidization. The effect of primary α spheroidization on the HCF properties is shown in Fig. 3. The increase, particularly in the HCF regimen, can be understood by recalling the refinement in the microstructure resulting from these treatments (compare Fig. 3 with Fig. 1a and c) and its accompanying decrease in slip length.

Table 2 Tensile properties of TIMET LCB (RX conditions)

Properties	E, GPa	YS, MPa	UTS, MPa	e_u, %	El, %	RA, %	$\varepsilon_F = \ln(A_0/A_F)$
RX	81	1110	1110	10.0	19.5	53.5	0.77
RX + 0.5 h 500 °C	106	1475	1565	3.6	7.6	20.7	0.23
RX + 4 h 500 °C	105	1440	1515	4.9	11.2	25.5	0.29
RX + PS	84	1270	1275	0.2	9.5	49.7	0.69
RX + PS + 0.5 h 500 °C	110	1665	1730	3.0	3.3	7.8	0.08
RX + PS + 4 h 500 °C	119	1400	1470	8.0	11.3	30.0	0.35
RX + PS + 0.5 h 525 °C	111	1595	1645	2.4	6.1	17.8	0.20
RX + PS + 0.5 h 550 °C	110	1495	1535	3.8	8.3	30.1	0.36

Note: PS, 10% tensile prestrain at room temperature

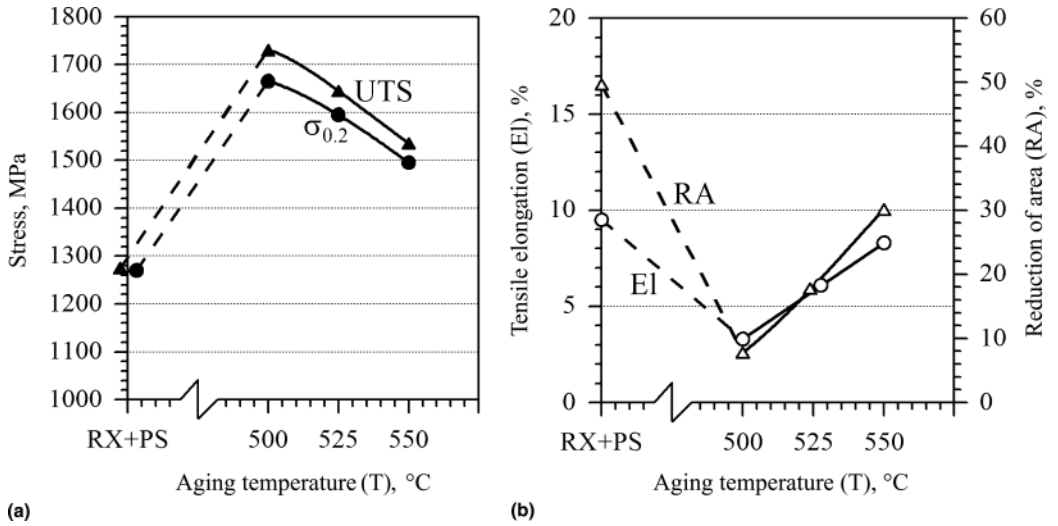

Fig. 2 Effect of aging temperature on the tensile properties of RX + PS material: (a) 0.2% YS and UTS; (b) El and reduction of area (RA)

3.3.2 Influence of Prestrain. The effect of PS on the HCF performance of RX TIMETAL LCB is illustrated in Fig. 4 and 5. Prestraining by 10% without subsequent aging led to a reduction in the HCF strength from about 680 MPa (RX) to 460 MPa (RX + PS), with this decrease occurring irrespective of the accompanying increase in YS from 1110 to 1270 MPa (Table 2). This effect is believed to be related to the exhaustion of work-hardening capability, as evidenced by the loss in uniform strain following the (RX + PS) treatment (Table 2).

Prestraining followed by aging for 0.5 h, when compared with aging without PS, resulted in a slight loss in HCF strength from 780 to 700 MPa (Fig. 5), although the former exhibited a YS that was approximately 200 MPa higher. This result can be attributed to the partial recovery of the uniform strain of the prestrained material during annealing at 500 °C for 0.5 h (Table 2).

3.3.3 Influence of Aging Temperature. The effect of aging temperatures from 500 to 550 °C on the HCF performance of RX and PS material is illustrated in Fig. 6. The highest HCF strength (700 MPa) was observed after aging at 500 °C. This aging temperature also resulted in the highest tensile YS (Table 2). Normalizing the HCF strengths by the tensile YS showed that aging at 525 °C resulted in the lowest HCF-to-YS ratio (0.38), while aging at 500 and 550 °C achieved a higher HCF-to-YS ratio (0.42).

3.3.4 Influence of Shot Peening on Surface Layer Properties. Examples of the changes in surface layer properties after SP (0.55 mmA) are shown in Fig. 7. Shot-peening resulted in an increase in surface roughness when compared with the EP reference (Fig. 7a). A slight increase in SP-induced microhardness was also observed; this low level was again attributed to the low-work-hardening capability of this condition (Fig. 7b). In contrast, high residual compressive stresses with a pronounced maximum below the surface were observed in these same regions. It should be noted that these residual compressive stresses are necessarily balanced by residual tensile stresses. Unfortunately, these residual tensile stresses in deep regions cannot be measured using the incremental hole-drilling method. The true residual stress-depth profile, as measurable by x-ray diffraction, is indicated by the dashed line in Fig. 7(c).

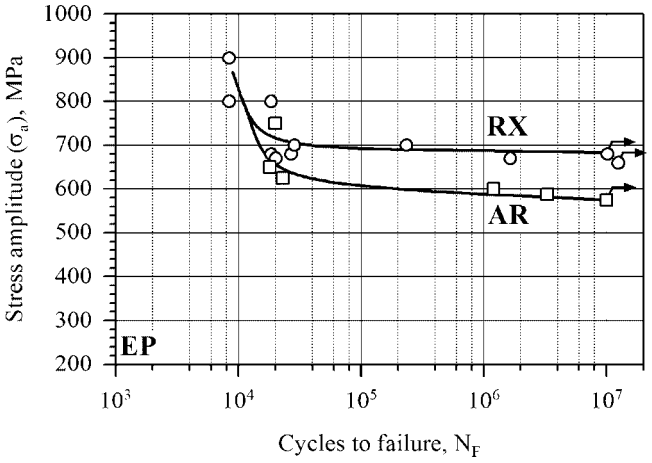

Fig. 3 S-N curves ($R = -1$) of AR and RX materials in EP condition

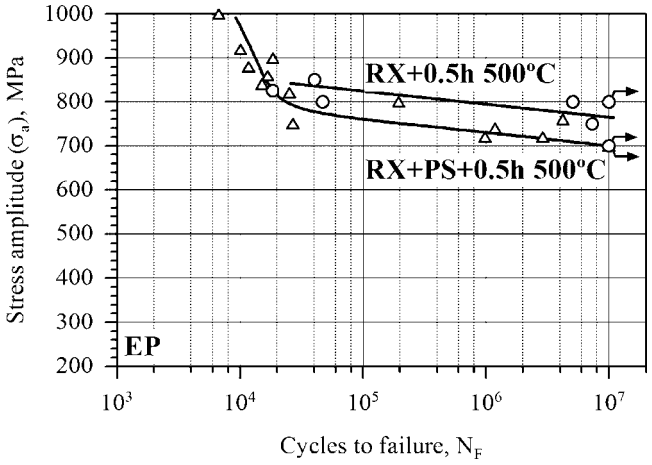

Fig. 5 S-N curves ($R = -1$) of RX materials and aged for 0.5 h at 500 °C and RX + PS materials and aged for 0.5 h at 500 °C in EP condition

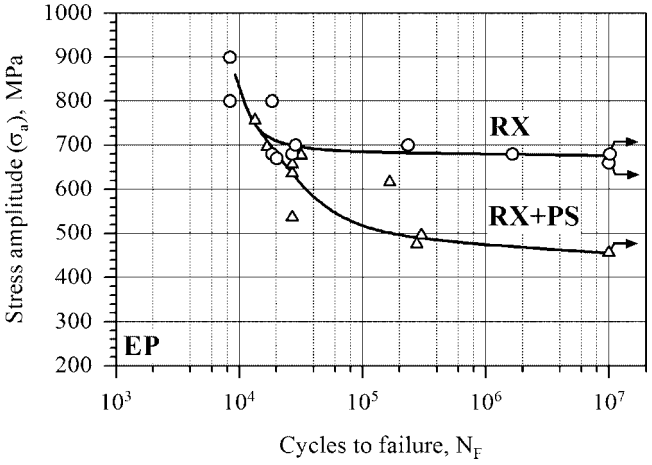

Fig. 4 S-N curves ($R = -1$) of RX and RX + PS materials in EP condition

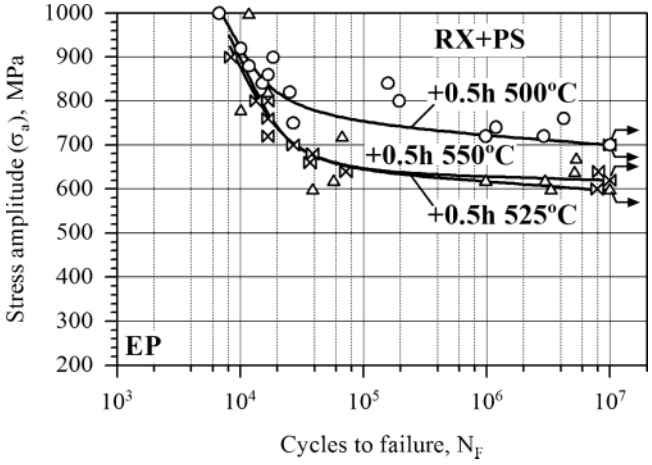

Fig. 6 S-N curves ($R = -1$) of RX + PS materials after aging at various temperatures in EP condition

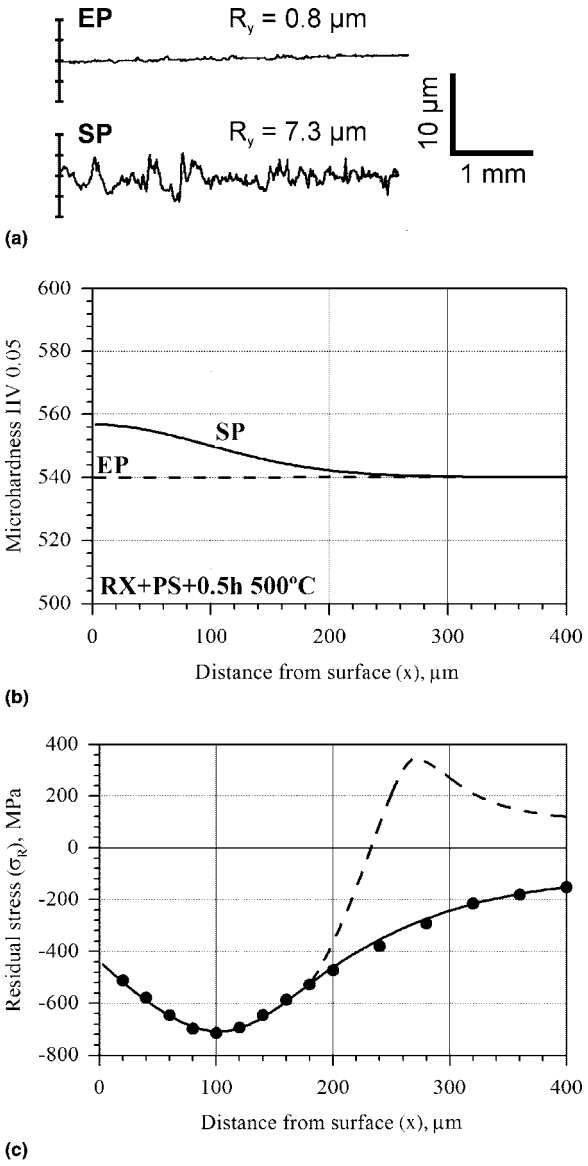

Fig. 7 Surface and surface layer properties after SP (RX condition + PS + aging for 0.5 h at 500 °C): (a) surface topography; (b) microhardness-depth profile; (c) residual stress-depth profile

3.4 High Cycle Fatigue Properties (Shot-Peened Conditions)

3.4.1 Influence of Prestrain. The effect of PS on the HCF performance of RX material after SP is illustrated in Fig. 8 and 9. Prestraining by 10% without subsequent aging led to a reduction in HCF strength after SP (i.e., 350 MPa [for RX material] to 300 MPa [for RX + PS material]). This decrease (Fig. 8) is lower than that observed in EP samples (220 MPa) (Fig. 4).

The effect of PS on the HCF strength of material aged for 0.5 h at 500 °C before SP is very similar to the effect of PS without aging (compare Fig. 9 and 8). Aging at 500 °C for 0.5 h reduced the HCF strength after SP from 520 MPa (no PS) to 400 MPa (with PS).

3.4.2 Influence of Aging Temperature. The effect of aging temperatures from 500 to 550 °C on the HCF performance of RX and PS material after SP is illustrated in Fig. 10. The highest HCF strength after SP was observed on material aged at 550 °C (550 MPa) followed by that on material aged at 525 °C (500 MPa). The lowest HCF strength after SP was found on material aged at 500 °C (400 MPa). Normalizing those HCF strengths by the tensile YS shows that aging at

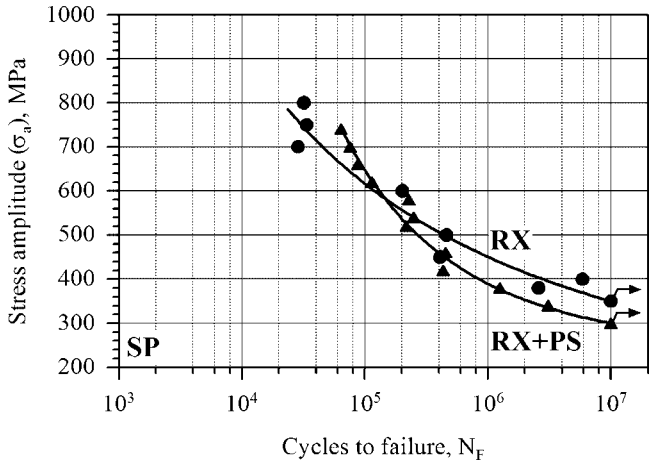

Fig. 8 S-N curves ($R = -1$) of RX and RX + PS materials in SP condition

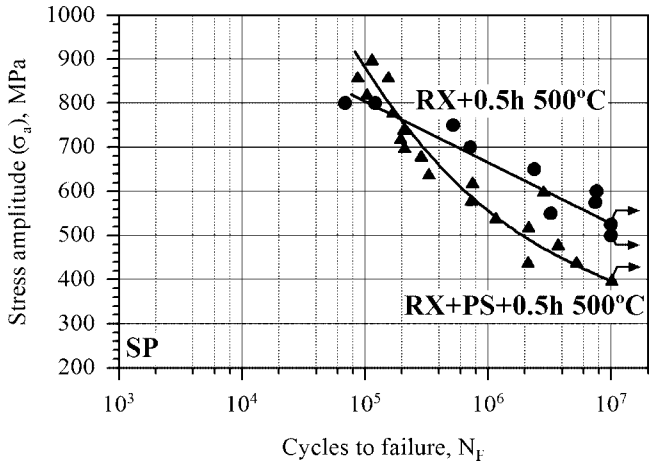

Fig. 9 S-N curves ($R = -1$) of RX and RX + PS materials after aging for 0.5 h at 500 °C in SP condition

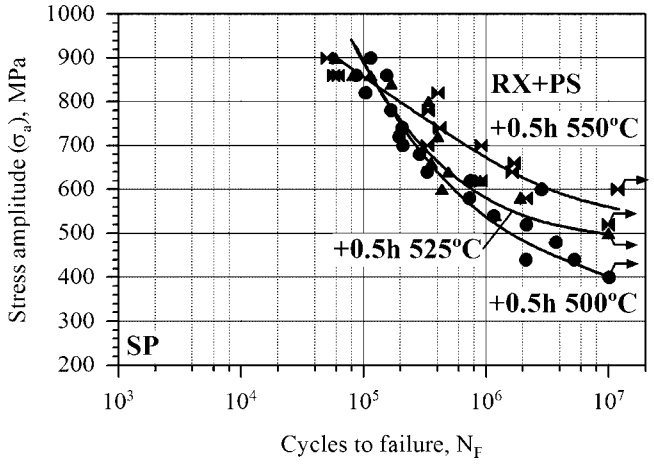

Fig. 10 S-N curves ($R = -1$) of RX + PS materials after aging at various temperatures in SP condition

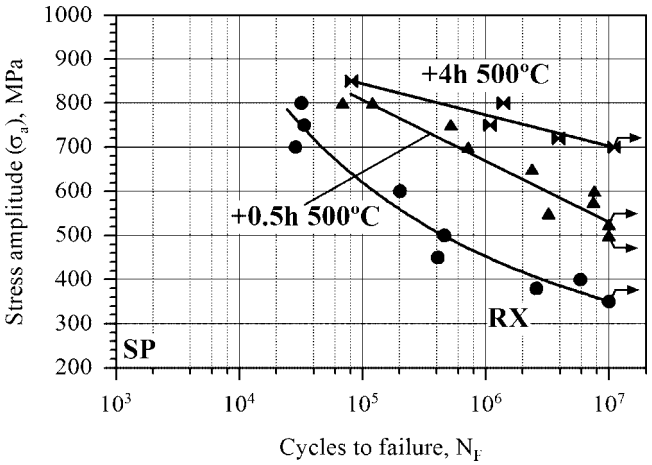

Fig. 11 S-N curves ($R = -1$) of RX materials aged at 500 °C in SP condition

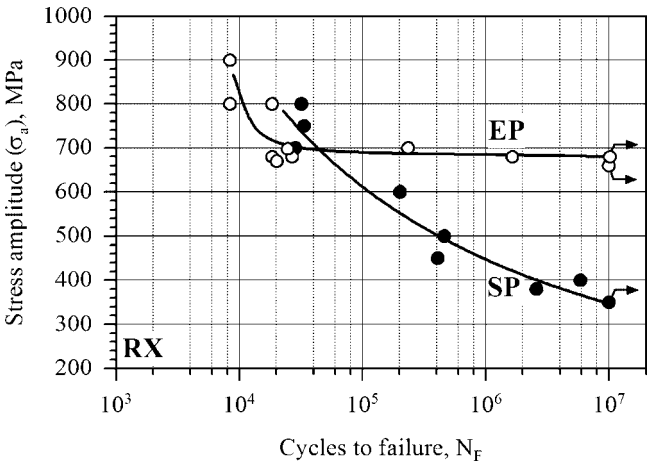

Fig. 12 S-N curves ($R = -1$) of RX materials in EP and SP conditions

500 °C resulted in the lowest HCF-to-YS ratio of 0.24. Increasing the aging temperature to 525 and 550 °C resulted in ratios of 0.31 and 0.37, respectively.

3.4.3 Influence of Aging Time. The effect of a variation in aging time from 0.5 to 4 h at an aging temperature of 500 °C is illustrated in Fig. 11. An increase in the aging time from 0.5 to 4 h at 500 °C increased the HCF strength after SP from 520 to 700 MPa. It appears that this effect can be associated, as previously noted, with an increase in the uniform strain and tensile ductility. The tensile yield and UTS were essentially unaffected by this increase in aging time (Table 2). Additional fatigue tests are underway to determine whether a similar pronounced effect of a variation in aging time also applies to prestrained material.

3.5 High Cycle Fatigue Properties (Shot Peening Versus Electropolishing)

3.5.1 Recrystallized Condition. The effect of SP on the HCF performance of the RX condition is illustrated in Fig. 12. This loss in fatigue strength was accompanied by the occurrence of subsurface fatigue crack nucleation, as opposed to surface crack nucleation, which is always observed on EP specimens. Typical fatigue crack nucleation sites are shown in Fig. 13.

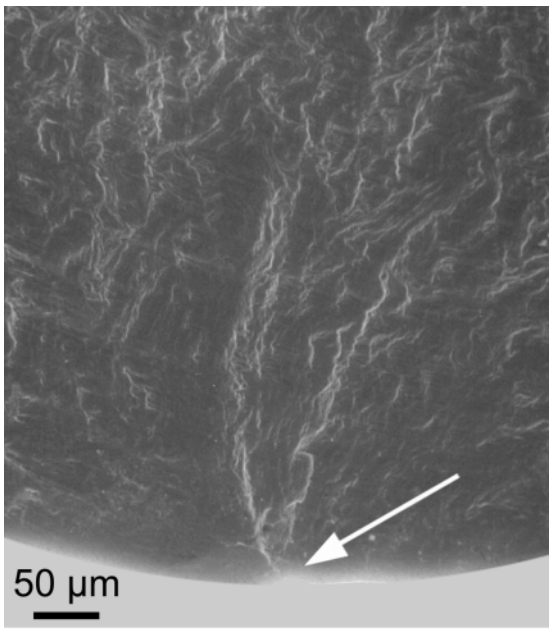

(a)

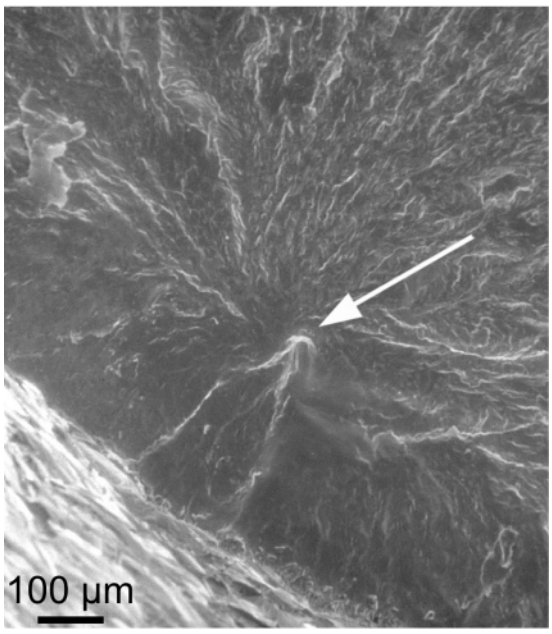

(b)

Fig. 13 Fatigue crack nucleation sites (SEM): (a) EP condition; (b) SP condition

These subsurface fatigue crack nucleation sites in SP specimens (Fig. 13b) are believed to be related to the high residual tensile stresses present at this depth (Fig. 7c).

3.5.2 Recrystallized Condition Plus Aging for 0.5 Hours at 500 °C. Aging at 500 °C for 0.5 h before SP did not alter the general trend (i.e., a drastic loss in HCF strength was observed if compared with the EP baseline) (Fig. 14). However, the corresponding strength values were 100 to 150 MPa higher than those observed on the RX condition (compare Fig. 14 with Fig. 12).

3.5.3 Recrystallized Plus Prestrained Condition. Shot-peening of RX + PS material significantly improved the fatigue life within the finite-life regimen (Fig. 15). However, a marked

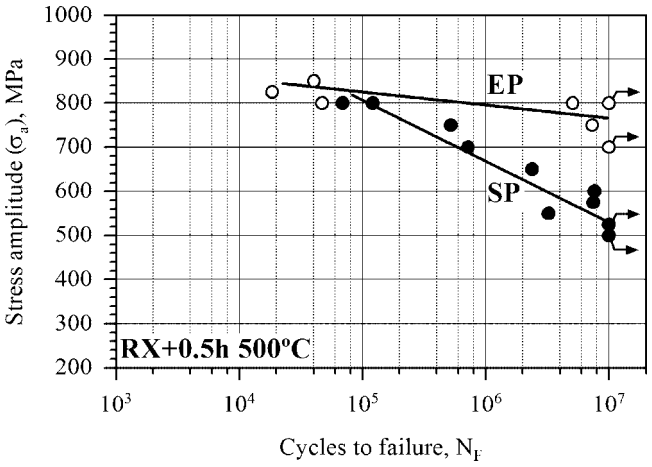

Fig. 14 S-N curves ($R = -1$) of RX materials and aged for 0.5 h at 500 °C in EP and SP conditions

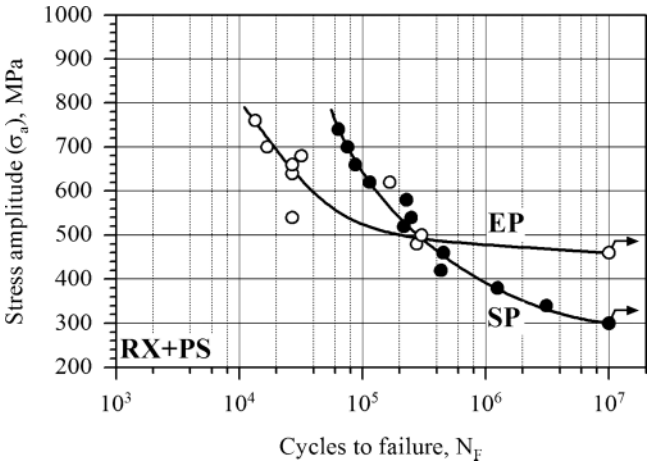

Fig. 15 S-N curves ($R = -1$) of RX + PS materials in EP and SP conditions

loss in the HCF strength was observed, which was very similar to the results from material without PS (compare Fig. 15 with Fig. 12).

3.5.4 Recrystallized Plus Prestrained Conditions Plus Aging for 0.5 Hours. Aging after PS was not found to alter the aforementioned effect of SP on fatigue performance. However, the degree of HCF strength reduction due to SP depended on the aging temperature (Fig. 16). For example, aging at 500 °C led to a loss of 300 MPa in the 10^7 cycles fatigue strength (Fig. 16a), while reductions of 100 and 50 MPa were observed after aging at 525 °C (Fig. 16b) and 550 °C (Fig. 16c), respectively.

Finally, the fatigue performance after roller-burnishing was similar to that after SP, with the HCF strength being reduced (Fig. 17), again, presumably, due to the high residual tensile stresses that led to subsurface fatigue crack nucleation.

4. Summary

Hot swaging followed by subtransus solution annealing resulted in a fine equiaxed β and spheroidized primary α microstructure in LCB. Compared with the as-received microstructure, consisting of elongated β grains and a semicontinuous grain boundary α layer, this microstructure was superior with regard to YS, true fracture strain, and HCF strength.

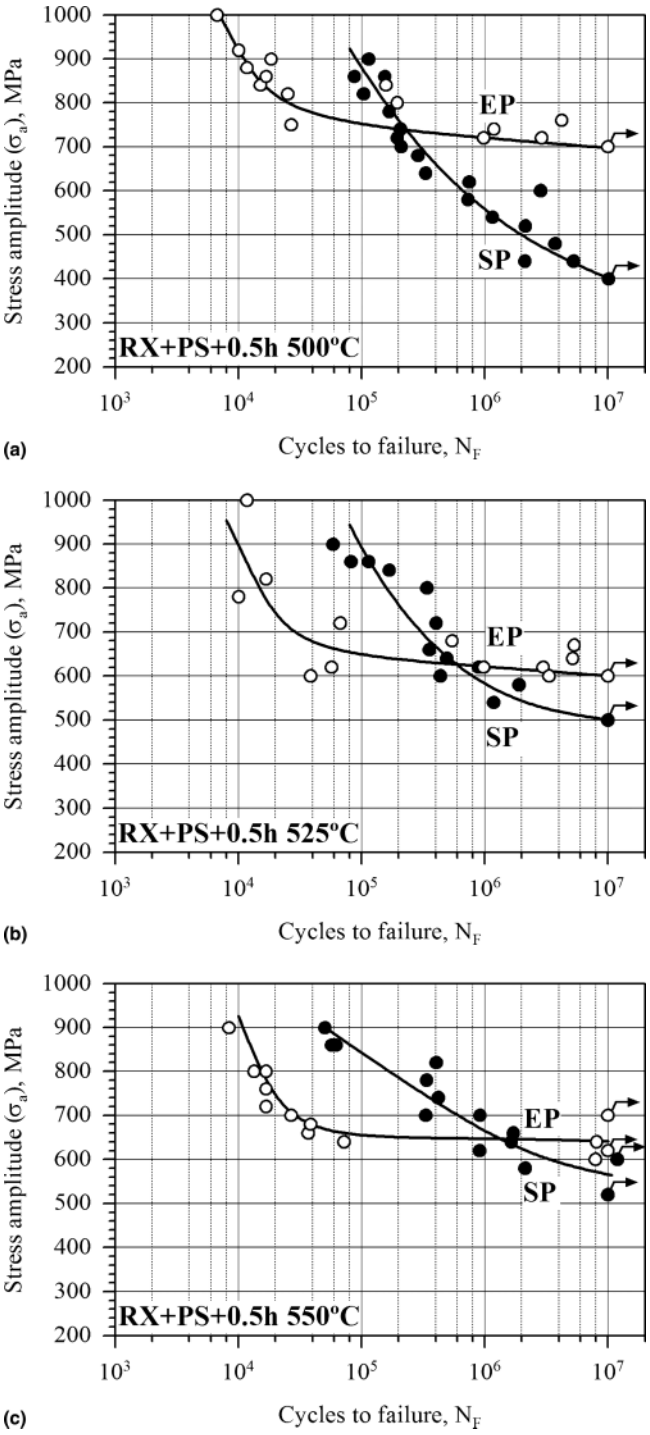

Fig. 16 S-N curves ($R = -1$) of RX + PS materials aged at various temperatures, and the effect of SP: (a) aged at 500 °C; (b) aged at 525 °C; (c) aged at 550 °C

A 10% straining before aging in the temperature range of 500 to 550 °C for 0.5 h markedly increased tensile YS and UTS values. However, the HCF strength was always lower if compared with the same aging cycles applied without PS. This effect was caused mainly by the already drastic loss in HCF

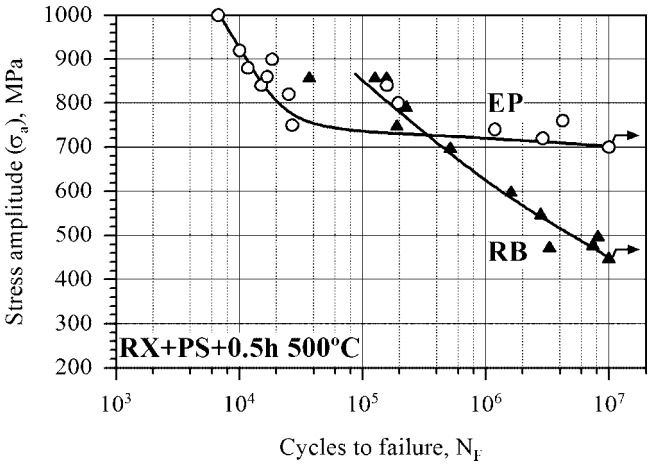

Fig. 17 S-N curves ($R = -1$) of RX + PS materials aged at 500 °C, and the effect of roller-burnishing (RB) versus EP

strength observed after PS without aging and is explained by the exhaustion of the work-hardening capability, as evidenced by the loss in uniform strain.

Shot-peening as well as roller-burnishing resulted in more or less marked decreases in HCF strength compared with the EP baseline. These losses in HCF strength were accompanied by subsurface fatigue crack nucleation caused by residual tensile stresses in these regions, which balance the outer compressive stress field.

Acknowledgments

The authors thank Mr. Yoji Kosaka of TIMET, Henderson, NV, for providing the TIMETAL LCB.

References

1. A. Sherman and S. Seagle, Torsional Properties and Performance of Beta Titanium Alloy Automotive Suspension Springs, *Beta Titanium Alloys in the 1980's,* R.R. Boyer and H. Rosenberg, Ed., The Materials Society, 1984, p 281-293
2. P.J. Bania, Beta Titanium Alloys and Their Role in the Titanium Industry, *Beta Titanium Alloys in the 1990's,* D. Eylon, R.R. Boyer, and D.A. Koss, Ed., The Materials Society, 1993, p 3-14
3. C. Sommer and D. Peacock, Mass Production Methods for Titanium Automotive Components, *Titanium '95,* P.A. Blenkinsop, W.J. Evans, and H.M. Flower, Ed., The University Press, Cambridge, 1996, p 1836-1843
4. P.G. Allen, P.J. Bania, A.J. Hutt, and Y. Combres, TIMETAL LCB: A Low Cost Beta Alloy for Automotive and Other Industrial Applications, *Titanium '95,* P.A. Blenkinsop, W.J. Evans, and H.M. Flower, Ed., The University Press, Cambridge, 1996, p 1680-1687
5. O. Schauerte, Titanium in Automotive Production, *Titanium and Titanium Alloys,* C. Leyens and M. Peters, Ed., Wiley-VCH, Weinheim, 2003, p 467-482
6. D. Kalish and H.J. Rack, The Structure and Properties of Thermomechanically Treated BETA-III Titanium, *Metall. Trans.,* Vol 3, 1972, p 1885-1892
7. A. Boettcher, Diploma thesis, Clausthal University of Technology, 2005
8. H. Kockelmann, Mechanical Methods of Determining Residual Stresses, Residual Stress Measurement, Calculation, Evaluation, V. Henk, H. Hougardy, and E. Macherauch, Ed., DGM Inform. Oberusel, 1990, p 37-52
9. H.J. Rack and T. Headley, Phase Transformations in Ti-3Al-8V-6Cr-4Zr-4Mo, *Metall. Trans. A,* Vol 10, 1979, p 909-920
10. S. Azimzadeh and H.J. Rack, Phase Transformations in Ti-6.8Mo-4.5Fe-1.5Al, *Metall. Trans. A,* Vol 29, 1998, p 2455-2467
11. J. Kiese, J. Zhang, O. Schauerte, and L. Wagner, Shot Peening to Enhance Fatigue Strength of TIMETAL LCB for Application as Suspension Springs, *Shot Peening,* L. Wagner, Ed., Wiley-VCH, Weinheim, 2003, p 380-385
12. M. Kocan, T. Ludian, M. Ishii, H.J. Rack, and L. Wagner, Optimization of Microstructure of TIMETAL LCB for Application as Suspension Springs, *LiMAT-2003,* W.E. Frazier, Y.D. Han, N.J. Kim, and E.W. Lee, Ed., Center for Advanced Aerospace Materials, Pohang University of Science and Technology, 2004, p 417-424